

GLOBAL AERO-STRUCTURAL DESIGN OPTIMIZATION OF COMPOSITE WINGS WITH ACTIVE MANEUVER LOAD ALLEVIATION

T. F. Wunderlich*, S. Dähne†, L. Reimer*, A. Schuster†

* German Aerospace Center (DLR), Institute of Aerodynamics and Flow Technology, Lilienthalplatz 7, 38108 Braunschweig, Germany

† German Aerospace Center (DLR), Institute of Composite Structures and Adaptive Systems, Lilienthalplatz 7, 38108 Braunschweig, Germany

Abstract

In the scope of the DLR project VicToria (Virtual Aircraft Technology Integration Platform), an integrated process for aero-structural wing optimization based on high fidelity simulation methods is continuously developed and applied. Based upon a parametric geometry, flight performance under transonic flight conditions and maneuver loads are computed by solving the Reynolds-averaged Navier–Stokes equations. Structural mass and elastic characteristics of the wing are determined from structural sizing of the composite wing box for essential maneuver load cases using computational structural mechanics. Static aeroelastic effects are considered in all flight conditions and active maneuver load alleviation is integrated in the process.

Global aero-structural wing optimizations are successfully performed for wings with and without active maneuver load alleviation. The active maneuver load alleviation is introduced with a simplified modeling of control surface deflections by using a mesh deformation technique. The minimization of the fuel consumption for three typical flight missions represents the objective function. Wing optimizations are performed for variable and constant planform parameters as well as for wings with conventional composite wing box structure and for more flexible wings. The latter is accomplished by introducing modifications of the structural concept and the strain allowable. A significant mass reduction of the optimized wing box is obtained for wings with active maneuver load alleviation, resulting in a drop in fuel consumption of about 3%. For wing optimizations with the more flexible wing concept the active maneuver load alleviation shows an additional reduction of the fuel consumption in the order of 2%. The wings with active maneuver load alleviation results in optimized wing geometries with increased aspect ratio and reduced taper ratio.

Keywords

Aero-Structural Design Optimization; Active Maneuver Load Alleviation; Composite Wing

NOMENCLATURE

A	aspect ratio
b	wingspan
c, c_{MAC}	chord, mean aerodynamic chord
g	acceleration of gravity
$n = L / (m g)$	load factor
$R = \sum R_i$	range (sum of mission segment ranges)
S	wing area
$t, t/c$	airfoil and relative airfoil thickness
x, y, z	coordinates
$\eta = 2y/b$	relative wingspan coordinate

Subscripts

CoG	center of gravity
CWB	center wing box
FS, MS, RS	front spar, middle spar, rear spar
HTP, VTP	horizontal tailplane, vertical tailplane
MG, NG	main gear, nose gear
WB	wing fuselage configuration

1. INTRODUCTION

The environmental impact of commercial aviation increases with the rapid growth of air travel and the CO_2 share of aviation will increase due to the increase of renewable energies in other transport sectors and in industry in general. For environmental protection and conservation of resources the main goal of the aeronautical research in Europe and in the United States of America is a strong reduction of the CO_2 emissions per passenger kilometer [1–4].

To achieve this challenging goal the development timescales for new technologies have to be reduced significantly. In this context the methodologies and processes for physics based aircraft design and optimization have to be improved. Furthermore, an assessment of new technologies with consideration of all relevant disciplines and their interactions on overall aircraft level will be essential in the future.

The efficiency of commercial aircraft is determined by aerodynamic performance in terms of lift to drag

ratio, aircraft empty mass, and thrust specific fuel consumption of the engine. For the accurate drag prediction under cruise flight conditions the flow physics of transonic and turbulent flow can be taken into account by using RANS-based computational fluid dynamics (CFD). To reduce the structural mass composite materials like carbon fiber reinforced polymers (CFRP) have been introduced in aircraft manufacturing. The corresponding structural concepts and sizing criteria have to be considered in the structural analysis and sizing process by using structural mechanics solvers based on the finite element method (FEM).

Within the aero-structural wing optimization the optimum trade-off between the aerodynamic performance and the wing mass is achieved through combining high fidelity methods for numerical flow simulation of the aircraft outer shape and structural sizing of the wing box with an appropriate optimization algorithm. Thereby, the interaction of aerodynamic forces and wing deformations have to be considered for accurate flight performance and static maneuver loads prediction by using fluid-structure coupling.

Wing design and optimization is a multidisciplinary task with a lot of practical constraints. For example, the size of the tail has to fulfill all stability and control constraints and thus depends on center of gravity range and wing geometry. Furthermore, the landing gear integration and the space allocation for the control surfaces including their actuators have to be considered. Neglecting the landing gear integration leads to unrealistic optimization results as shown in [5].

The technology of active maneuver load alleviation (MLA) reduces the aerodynamic loads by using trailing edge control surface deflections to adapt the lift distribution under maneuver flight conditions. This technology has been published by White [6] for example and successfully applied to the Lockheed L-1011 [7]. In modern airliners, the maneuver load alleviation functions are an integral part of the flight control system. The active and passive load alleviation technologies have to be integrated into the sizing process of the aircraft structure and result in longer maintenance intervals and mass reductions. Therefore, a physical modeling of active maneuver load alleviation technology is pursued in preliminary aircraft design.

With increasing knowledge of composite materials further mass reduction potentials can be exploited by better adaptation of fiber direction to internal loads, introduction of advanced structural concepts, and new manufacturing processes. The more flexible wing concept is a result of mass reduction due to new structural concepts with increased strain allowable and applied to the current generation of aircraft from Boeing (Boeing 787 and Boeing 777-8/9). In addition the passive load alleviation due to static aeroelastic effects leads to further wing mass reduction.

Improvements in automation and coupling of accurate simulation methods in combination with advances in

numerical optimization strategies lead to the emergence of multidisciplinary design optimization (MDO) based on high fidelity methods. The challenge in using MDO based on high fidelity methods is the large number of design parameters and constraints and the increased computing effort. To overcome this issue, the adjoint method enables the efficient calculation of the flow variable gradients as a function of the design parameters for gradient based optimization [8, 9]. Up-to-date applications of the adjoint approach for multidisciplinary wing optimization have been shown in the publications of Kenway and Martins [5]; Liem, Kenway, and Martins [10]; Keye et al. [11]; and Abu-Zurayk et al. [12]. These publications show that the gradient based optimization using the adjoint approach is an adequate method for multidisciplinary wing optimization with high fidelity simulation programs and a large number of design parameters.

In this work an alternative MDO approach is introduced for cases in which gradients cannot be computed efficiently for all relevant disciplines. This applies particularly to cases which involve CAD modeling and structural sizing of composite structures using proprietary codes. Additionally, the gradients based approaches have to be reconsidered for flows near the maximum lift including flow separations and the usage of active control surface deflections. Furthermore, a certain degree of flexibility in the process architecture and optimization strategy is desired. Especially the option to use optimization strategies seeking for the global optimum is important.

2. METHODS

In the DLR project VicToria [12–17], an integrated process for aero-structural wing optimization based on high fidelity simulation methods is continuously developed and improved. A detailed description of the original process chain and their successful application is published by Wunderlich et al. [18, 19]. The improvements relate to the introduction of grid deformation techniques for large geometry changes and simplified control surface deflections. Further extensions include a landing gear integration, a tail sizing based on handbook methods and a trim drag estimation functionality.

The MDO architecture of the integrated process chain falls in the category of MDF optimizations (Multi-Disciplinary Feasible) and can be described as ASO (Asymmetric Subspace Optimization) according to Martins and Lambe [20].

A detailed description of the process chain is outlined in the publication of Wunderlich et al. [21] and only the top level is presented here again.

2.1. Process chain for aero-structural wing optimization

The process chain applied is illustrated in terms of XDSM-diagrams (Extended Design Structure Matrix) [22]. Each component in the diagram receives input data in vertical direction and provides output data in horizontal direction. Input and output data are marked by parallelograms. Thick gray lines show the data flow, and thin black arrows indicate the process flow. The numbering system defines the order in which the components are executed.

The flow chart of the process chain for aero-structural wing optimization is shown in FIG. 1. In every optimization step, the geometrical aircraft description of the baseline configuration is recalculated and updated in accordance with the current values of the design parameters. The resulting aircraft geometry is transferred to the subsequent simulation programs by using the Common Parametric Aircraft Configuration Schema (CPACS) [23, 24]. The recalculation of the aircraft geometry includes the wing positioning relative to the fuselage, the integration of the main landing gear, the sizing of the tail, and the check of geometrical constraints.

In the next step the parametric CAD model is updated, the aerodynamic volume mesh is deformed, and the structural model is generated. The parametric CAD model has been built in the commercial software CATIA® V5, which enables accurate surface representation, and robust and time efficient geometry changes.

Within the CFD volume mesh deformation process, the mesh representing the baseline configuration is deformed in two stages for all flight conditions in parallel. In the first stage, the geometrical changes between the baseline and the current geometry are computed based on the corresponding structured multi-block (SMB) surface meshes. The latter result from the automatic surface mesh generation and have an identical mesh topology with the same number of points. For automatic surface mesh generation, the commercial software Pointwise® is applied. In the second stage, the control surface deflections are taken into account. Corresponding to the control surface deflection to be produced, the surface mesh displacement field is computed for each flight condition. It is propagated to the CFD volume mesh by using the Elasticity Analogy (EA) mesh deformation method [25] available in the FlowSimulator [26–28] environment.

For the generation of the structural model the DLR in-house tool DELiS (Design Environment for thin-walled Lightweight Structures) [29] is used. Based on the central data format CPACS, DELiS automatically generates a consistent finite element mesh by using the open-source tool Gmsh [30]. The finite element model is made up of shells elements enriched with physical properties of the wing spars, ribs, and skin cells and finally exported for the commercial FE solver MSC Nastran™.

The fluid-structure coupling loop is marked with a rounded yellow box and the values of the design mission lift-to-drag ratio, the wing mass and the objective function value are evaluated for the convergence examination. The fluid-structure interaction belongs to the category of loosely coupled analysis [31, 32], with the main difference of replacing the structural analysis of a sized wing structure by a combined structural wing analysis and sizing process. The integration of the structural sizing process into the fluid-structure coupling loop reduces the number of iterations by introducing a damper like behavior.

For all flight conditions the aerodynamic forces and coefficients are computed using RANS-based CFD simulations. The flow simulations are performed by using the DLR TAU-Code [33, 34] which is integrated in the HPC framework FlowSimulator [26]. The solver's capabilities with respect to accurate flow predictions, also in near off-design regions, have been demonstrated in numerous publications, including those of the AIAA Drag Prediction Workshop Series [35]. The approach ensures that flight performance under cruise flight conditions and selected maneuver loads with consideration of flow separations are analyzed accurately and efficiently.

Based on the aerodynamic loads computed for the flight conditions considered, the wing-box structure is sized. Within the structural analysis and sizing process the objective is to fulfill the structural constraints in terms of failure criteria and converge the margins of safety (MoS) and wing mass. Different design criteria are applied to ensure a valid structural design. As proposed by Dähne et al. [36] for stiffened panels, the criteria for strength, maximum strain, and local and global buckling are used for skin and all stringer components. The main results of this process are the wing mass and the deformed wing shapes for the flight conditions considered. The structural analysis and sizing process uses the commercial software MSC Nastran™ for computing the internal loads and stresses. The commercial software HyperSizer® is applied for sizing the composite wing box.

The structural deformations form the input for the CFD volume mesh deformation. The mesh deformation method based on radial basis functions (RBF) [37] available in the FlowSimulator is used. Afterwards, the objective function is evaluated and the convergence criteria of the static aeroelastic analysis are examined. Once convergence of the fluid-structure coupling loop is reached, the objective function value is given to the global optimizer.

After the optimization run has finished the optimized vector of design parameters represents the main result of the process chain for the corresponding optimization problem.

2.2. Global optimization strategy

For the wing optimizations a surrogate based optimization (SBO) method [38] has been selected. This global optimization strategy represents an adequate

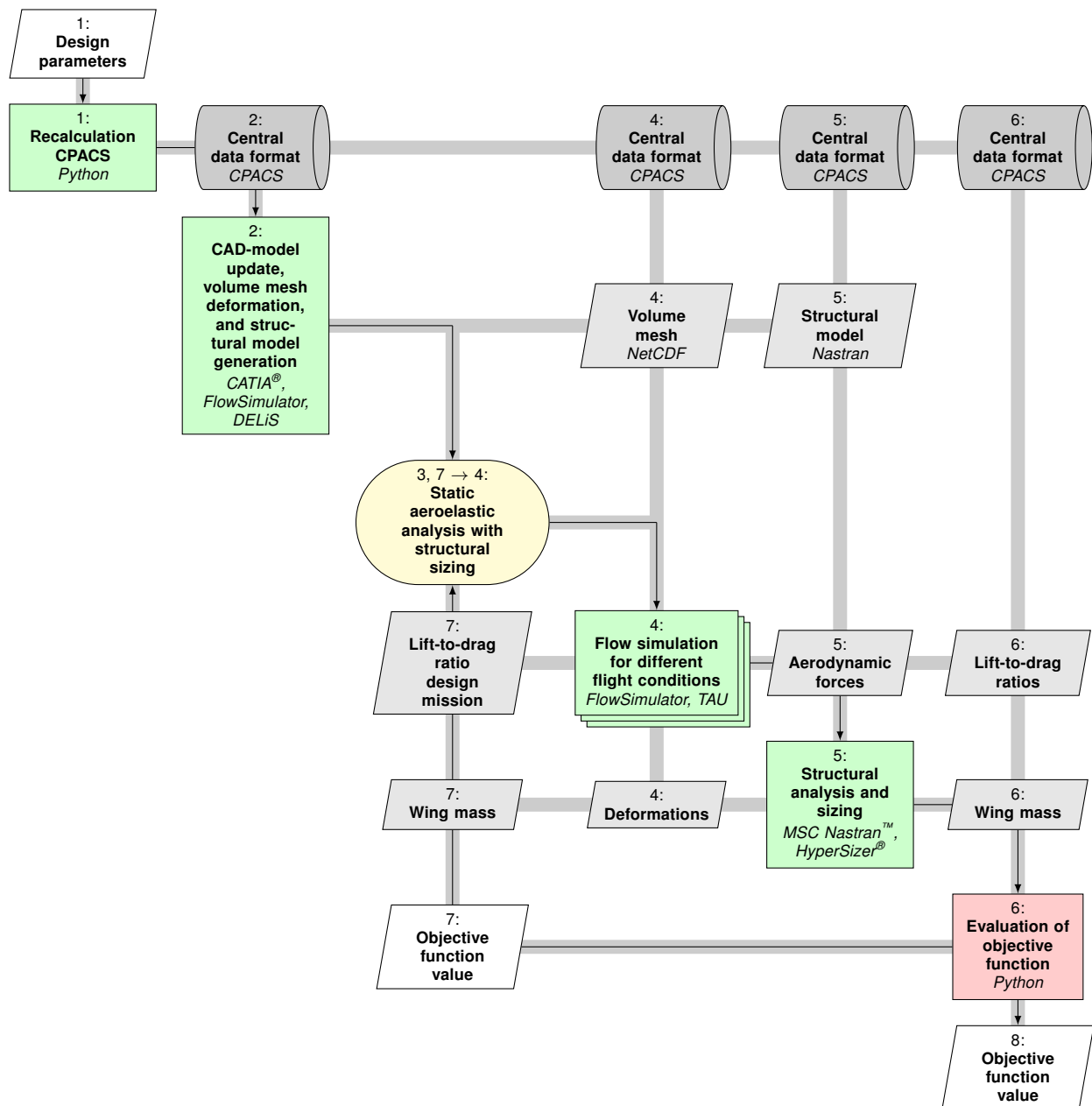


FIG 1. Flow chart of the process chain for aero-structural wing optimization.

compromise between exploring the design space and locating the optimum.

The selected optimization method is an implementation of the optimization method EGO (Efficient Global Optimizer), which has been introduced by Jones et al. [39] and is discussed in Forrester et al. [40]. At the beginning of the optimization a design of experiments (DoE) for a selected number of samples is performed. For the calculated objective function value and for each selected constraint a surrogate model based on kriging [41] is built. These surrogate models are able to model the nonlinear behavior of the objective and constraints. Additionally, a statistical error estimation is included.

Based on the surrogate models of the objective function and constraints, a hybrid optimization strategy is used to find the optimum in terms of expected improvement (EI), which combines the predictions

of objective function value and model error. The hybrid optimization strategy starts with a global optimization method and the localization of the optimum is improved by the application of a local optimization method. For the resulting global optimum in terms of expected improvement a recalculation with the physical model is performed. The result of this recalculation is then used to improve the surrogate models for the objective function value and constraints. The described optimization procedure is iterated until convergence is reached.

2.3. Active maneuver load alleviation

The active maneuver load alleviation (MLA) reduces the aerodynamic loads by using trailing edge control surface deflections to adapt the lift distribution under maneuver flight conditions. In a pull up maneuver for

example, an inboard load shift can be achieved by increasing the lift in the inboard region with positive control surface deflections and decreasing the lift in the outboard wing region with negative control surface deflections. The result of the inboard load shift are reduced aerodynamic loads in terms of wing bending moment. Thereby, the inboard load shift is related to a forward shifting of the center of pressure in the case of backward swept wings and the aircraft trimming redistributes the lift between the wing and the horizontal tail. As a result, the lift of the horizontal tail increases and simultaneously the lift of the wing decreases.

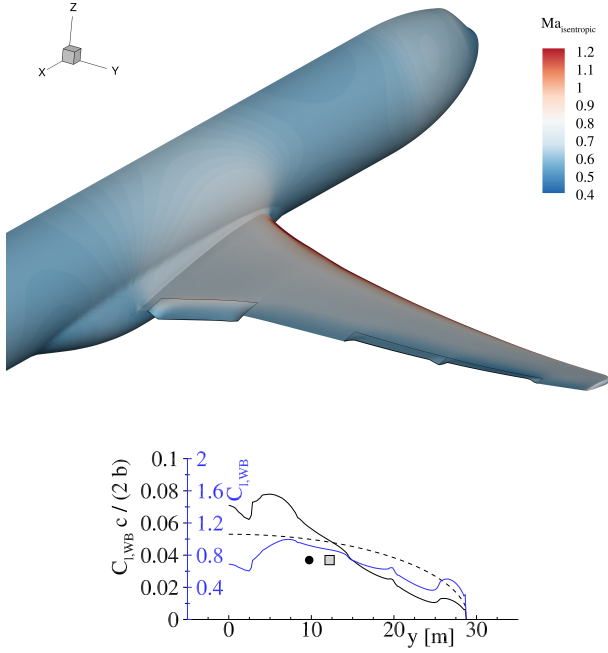


FIG 2. Maneuver load alleviation.

The aerodynamic limits of the lift distribution adaptation are the minimum and maximum local lift coefficients with deflected control surfaces. These limits can be explained with flow separations, which occur in a viscous fluid with adverse pressure gradient. Furthermore, the geometrical extension of the control surfaces are limited by the rear spar position of the wing box and the required actuator size, mass, and actuation power.

In this work the control surface deflections are modeled by using a mesh deformation approach. This approach allows the consideration of viscous flow effects including flow separation in the aerodynamic loads computation, but neglects the complex flow physics around the edges of the deflected control surfaces.

In FIG. 2 the surface solution for a pull up maneuver with control surface deflections for active maneuver load alleviation is shown. The corresponding lift- and lift coefficient distribution with the center of lift (black dot) are presented on the lower part of the figure. Furthermore, the elliptical lift distribution (dashed line) with its center of lift (gray square) is shown as reference. With the consideration of active maneuver load alleviation further wing box mass reduction and fuel consumption reduction will be expected.

2.4. Structural concept of the more flexible wing

For the more flexible wing the structural concept and the maximum strain allowable have been changed. The structural concept of the conventional composite wing structure consists of classical upper skin ply share and blade stringers. For the strain allowable a conservative value of $3500 \mu\text{m}/\text{m}$ has been selected as proposed in Military Handbook [47]. Through a detailed consideration of stringer constraints and stiffness, the evaluation of a more flexible wing becomes possible, while relevant structural constraints are considered. For stiffened composite panels the more flexible wing concept has been investigated by Bach and Hühne [48].

In this work, the more flexible wing has been modeled with a stringer dominant structural concept of the upper cover. This includes a selected upper skin percentage ply share of (10/80/10) and the usage of I-stringers. Based on the modified structural concept a value of $5000 \mu\text{m}/\text{m}$ has been selected for the strain allowable of the more flexible wing. The percentage ply share of the lower skin, spars, and ribs has been optimized in a preceding aero-structural wing optimization [21] and the values has been transferred to the presented optimizations with more flexible wings. In TAB. 1 the differences between the structural concepts of the conventional composite wing and the more flexible wing have been summarized.

		Structural concept of conventional composite wing	Structural concept of more flexible wing
Structural concept of the upper covers		Skin dominated design	Stringer dominated design
Stringer type		Blade stringer	I-stringer
Strain allowable	ε	$3500 \mu\text{m}/\text{m}$	$5000 \mu\text{m}/\text{m}$
Upper skin percentage ply share center wing box	$0^\circ / \pm 45^\circ / 90^\circ$	70/20/10	10/80/10
Upper skin percentage ply share inboard	$0^\circ / \pm 45^\circ / 90^\circ$	60/30/10	10/80/10
Upper skin percentage ply share mid wing	$0^\circ / \pm 45^\circ / 90^\circ$	60/30/10	10/80/10
Upper skin percentage ply share outboard	$0^\circ / \pm 45^\circ / 90^\circ$	40/50/10	10/80/10

TAB 1. Structural concept overview.

3. RESULTS

In the DLR project VicToria multi-mission aero-structural wing optimizations have been successfully applied to optimize wing planform, twist, and thickness distribution of the Airbus XRF1 research configuration. To investigate the impact of active maneuver load alleviation, the optimizations have been performed for wings with and without the consideration of active maneuver load alleviation. Thereby, the XRF1 is an Airbus provided industrial standard multi-disciplinary research testcase representing a typical configuration for a long range wide body aircraft.

In the first step, the wing optimizations without consideration of active maneuver load alleviation have been performed. The result of the twist and thickness distribution optimization represents the baseline. With the optimization of wing planform, twist, and thickness distribution, the design space has been further extended and shows the full potential of multidisciplinary wing optimization with the introduced optimization approach. Additionally, a result for the optimization of wing planform, twist, and thickness distribution for a more flexible wing by changing the structural concept and the maximum strain allowable is presented.

In the next step the active maneuver load alleviation has been introduced by using active control surface deflections in all maneuver load cases. Thereby, the control surface deflection angles have been used as additional design parameters. In these wing optimizations the wing planform, twist, and thickness distribution have been optimized for wings with conventional composite wing structure and for a more flexible wing, respectively.

3.1. Design task

The design task describes the objective function, the design space, and the constraints. In this work the wing design for a long range commercial aircraft configuration has been selected.

3.1.1. Objective function, flight missions, and load cases

The objective function of the multi-mission aero-structural wing optimizations is the combined fuel consumption of three selected flight missions. In this work, the fuel consumption is defined in terms of fuel burn per range and payload. Hence, the combined fuel consumption is the weighted sum of the corresponding mission fuel consumption as given in Eq. (1).

$$(1) \quad \frac{m_F}{R m_P} = \sum_i w_i \left(\frac{m_F}{R m_P} \right)_i$$

In TAB. 2 an overview of the selected flight missions and weight factors is shown. With the selected

weighting factors the expected relative frequency of the missions in operation has been considered.

For the study and design mission the design Mach number of the Airbus XRF1 has been selected. The design mission range is set to 6500 nm and the corresponding payload is a result of the aero-structural wing analysis. The selection of range and payload for the study mission is based on a typical long range mission with a load factor of 0.85 and represents the mission for which the aircraft will be optimized primarily. The difference between high speed and the study mission is the increased cruise Mach number to consider off-design conditions in the wing optimization. For the structural sizing of the wing box the maneuver load cases with the maximum loads have to be defined. These maneuver load cases have been derived from the flight envelope limits and the limits of the maneuvering load factor resulting from the certification regulations CS-25/FAR 25. In TAB. 2 an overview of the selected maneuver load cases is given.

To compute the fuel consumption of each flight mission a modeling from conceptual design [42, 43] has been used. Thereby, the flight mission has been divided into five segments and the corresponding aircraft mass fractions have been transferred from typical values given in the textbook published by Jenkinson [44] to the Airbus XRF1 reference aircraft configuration. The flight mission segments are summarized in TAB. 3.

For the cruise segment of the flight mission a constant Mach number and constant lift-to-drag ratio have been assumed. Furthermore, the thrust specific fuel consumption has been modeled by a formula published by Mattingly [45]. This formula describes the dependency of the thrust specific fuel consumption from the flight conditions for a given engine and has been adapted to a typical engine map in the Rolls-Royce Trent 1000 class. The formula with the adopted parameters are given in Eq. (2).

$$(2) \quad TSFC = \frac{C_1 + C_2 Ma}{g} \sqrt{\frac{\theta}{\theta_{SL}}}$$

with $C_1 = 0.245 \text{ h}^{-1}$ and $C_2 = 0.415 \text{ h}^{-1}$

The aircraft mass fraction for the cruise segment is calculated with Eq. (3), which has been derived from the well-known Breguet range equation and the thrust specific fuel consumption of Eq. (2).

$$(3) \quad R_{23} = \underbrace{\sqrt{\kappa R \theta_{SL}}}_{\text{const.}} \frac{Ma}{C_1 + C_2 Ma} \frac{L}{D} \ln \frac{m_2}{m_3}$$

with $\kappa = 1.4$,

$$R = 287.05 \text{ m}^2/(\text{s}^2 \text{ K}),$$

$$\theta_{SL} = 288.15 \text{ K}$$

For each flight mission the corresponding lift-to-drag ratio for the cruise segment is a result of the aerodynamic coefficients of the flow simulation for the wing

			Study mission	High speed mission	Design mission
Flight missions	Weight factor	w_i	0.6	0.1	0.3
	Cruise Mach number	Ma	0.83	0.85	0.83
	Range	R	4000 nm (7408 km)	4000 nm (7408 km)	6500 nm (12 038 km)
	Payload	m_P	40 800 kg	40 800 kg	-
	Reserve fuel ratio	$m_{F,res}/m_F$	0.1410	0.1410	0.0950
			Pull up maneuver	Push over maneuver	Roll maneuver
Load cases	Altitude	H	0 m	6096 m	0 m
	Mach number	Ma	0.552	0.784	0.552
	Lift coefficient wing fuselage	$C_{L,WB}$	0.739	-0.319	0.493
	Load factor	n	2.5	-1.0	1.667

TAB 2. Flight missions and load cases.

Segment number	Mission segment	Aircraft mass fraction	Reference
1	Taxi and take-off	$m_1/m_{TO} = 0.997$	[44]
2	Climb and accelerate	$m_2/m_1 = 0.981$	[44]
3	Cruise	$m_3/m_2 = \exp\left(-\frac{(C_1+C_2 Ma) R_{23}}{\sqrt{\kappa R \theta_{SL} Ma L/D}}\right)$	Eq. (3)
4	Descent for landing	$m_4/m_3 = 0.998$	[44]
5	Landing and tax	$m_5/m_4 = 0.997$	[44]

TAB 3. Flight mission segments.

body configuration, the estimated aerodynamic coefficients of the tail, and the given residual drag coefficient as shown in Eq. (4).

$$(4) \quad \frac{L}{D} = \frac{C_L}{C_D} = \frac{\overbrace{C_{L,WB} + C_{L,HTP}}^{\text{flow simulation}}}{\underbrace{C_{D,WB} + C_{D,HTP} + C_{D,VTP} + C_{D,res}}_{\text{flow simulation}} + \underbrace{C_{D,res}}_{\text{const.}}}$$

The lift coefficient of the horizontal tail is a result of aircraft trimming for the prescribed center of gravity position. This aircraft trimming loop based on the equilibrium of forces and moments around the center of gravity is not described in detail here. For the drag coefficient prediction of the tail a simplified approach from conceptual design [46] based on Prandtl's lifting-line theory and flat plate analogy has been used.

The take-off mass of the aircraft is the sum of the residual mass m_{Res} (structural mass without the wing and tail including the operating items mass), the wing mass m_W , the tail mass, the payload, and the fuel masses (mission and reserve fuel) as shown in Eq. (5).

$$(5) \quad m_{TO} = \overbrace{m_{Res} + m_W + m_{HTP} + m_{VTP}}^{\text{operating empty mass } m_{OE}} + m_P + m_F + m_{F,res}$$

The wing mass is a result of the structural sizing of the wing box and the tail mass is estimated by scaling the tail mass of the reference aircraft with the tail surface ratio after tail sizing. Thereby, the tail sizing

based on conceptual design methods by using constant tail volume coefficients [43]. The fuel mass follows directly from the aircraft mass difference for the complete flight mission.

For the calculation of the fuel consumption the required equations are listed in TAB. 4. Thereby, the fuel mass ratio m_F/m_{TO} is computed from the aircraft mass fractions with the given range R and the lift-to-drag ratio L/D for the cruise segment. For the study mission and the high speed mission the payload is specified and the take-off mass has to be calculated. In the design mission the take-off mass equals the maximum take-off mass and the payload is resulting from the cruise flight performance and wing mass. For both cases the corresponding equations are evaluated in terms of the payload ratio m_P/m_{TO} . With the fuel mass ratio and the payload ratio the fuel consumption per range and payload follows directly from the last equation in TAB. 4.

3.1.2. Design parameters and constraints

The outer shape of the wing has been parameterized with the design parameters shown in FIG. 3.

Thereby, the wing planform is calculated from wing area, aspect ratio, leading edge sweep angle, and the taper ratios of the inboard, mid wing, and outboard wing region. Furthermore, the twist and relative thickness distribution are defined in the corresponding wing sections. In the wing sections between these sections the values of the twist and relative thickness are interpolated linearly. The fuselage shape has been held constant during the wing optimizations. For the belly fairing an adaptation to the root section of the wing has been considered by scaling the middle

$$\text{Fuel mass ratio} \quad \frac{m_F}{m_{TO}} = 1 - \frac{m_1}{m_0} \frac{m_2}{m_1} \frac{m_3}{m_2} \frac{m_4}{m_3} \frac{m_5}{m_4}$$

$$\text{Payload ratio} \quad \frac{m_P}{m_{TO}} = 1 - \frac{m_{OE}}{m_{TO}} - \left(1 + \frac{m_{F,res}}{m_F}\right) \frac{m_F}{m_{TO}} \quad \text{for specified } m_{TO} \text{ and variable } m_P$$

$$\frac{m_P}{m_{TO}} = \frac{1 - \left(1 + \frac{m_{F,res}}{m_F}\right) \frac{m_F}{m_{TO}}}{m_{OE} + m_P} m_P \quad \text{for specified } m_P \text{ and variable } m_{TO}$$

$$\text{Fuel consumption} \quad \frac{m_F}{R m_P} = \frac{m_F}{m_{TO}} \frac{m_{TO}}{m_P} \frac{1}{R_{12} + R_{23} + R_{34}}$$

TAB 4. Used formulas for the computation of the fuel consumption.

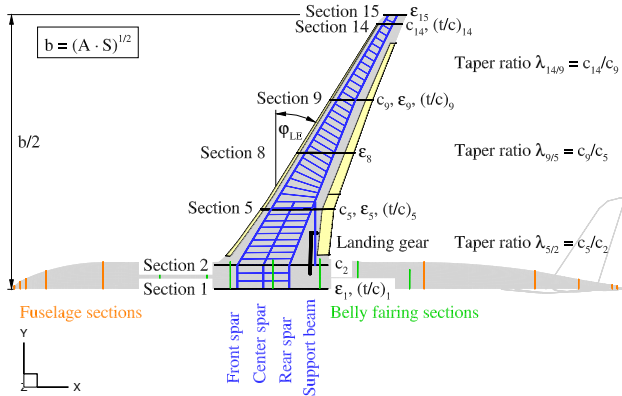


FIG 3. Outer shape design parameters.

section of the belly fairing. The positioning of the wing in x-direction has been performed by maintaining the x-position of the aerodynamic center. The wing box regions and the global wing box design parameters are shown in FIG. 4.

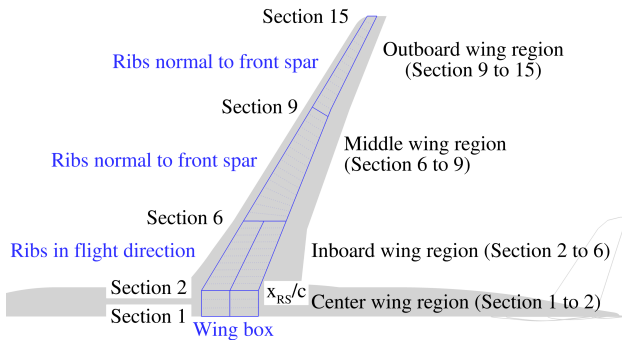


FIG 4. Wing box regions and design parameters.

Thereby, the wing box has been separated into four regions for which the percentage ply share of the lower skin, spars, and ribs has been optimized for the more flexible wing concept in a preceding aerostructural wing optimization as mentioned before. The definition of the spars is based on the relative positioning of spar points, which are given in relative span and relative chord coordinates. For the ribs a constant rib spacing has been considered. In the

center wing and inboard region the ribs are oriented in flight direction and in the middle and outboard wing region the ribs are positioned normal to the front spar. These rib orientations are typical for Airbus aircraft. In TAB. 5 all selected global design parameters are summarized.

The definition of the control surfaces and the fuel tanks are shown in FIG. 5. For the consideration of the active maneuver load alleviation the deflections of the inboard flap, outboard flap and outboard aileron have been used as global design parameters in the corresponding wing optimizations.

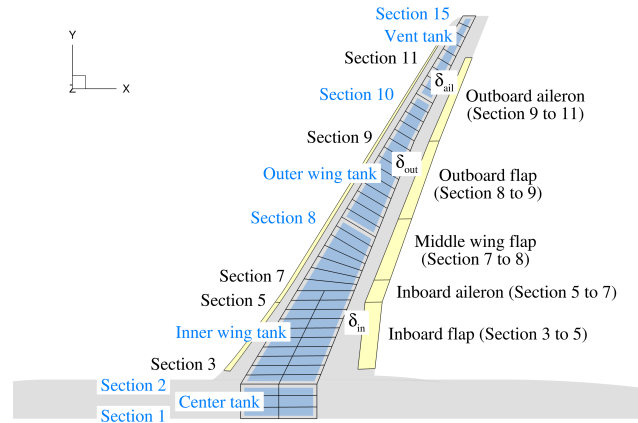


FIG 5. Definition of control surfaces and fuel tanks.

During the wing optimization the required fuel tank volume is calculated for all selected flight missions and compared with the useable fuel tank volume. The fuel tank volume constraint has been considered in all wing optimizations.

With the consideration of geometry constraints for the integration of a landing gear and the control surfaces, a better comparability of the optimization results with the baseline aircraft configuration is achieved. FIG. 6 gives an overview of the geometrical constraints, which have to be fulfilled for each wing design. This includes the positioning of the main gear wheel on the ground with a given relative x-position while maintaining the minimal allowed distances between the main landing gear, the control surfaces, and the wing box.

In FIG. 7 further geometrical constraints for the landing gear integration are shown.

Design parameters	Wing area	S
	Aspect ratio	A
	Leading edge sweep angle	φ_{LE}
	Taper ratio inboard	$\lambda_{5/2}$
	Taper ratio mid wing	$\lambda_{9/5}$
	Taper ratio outboard	$\lambda_{14/9}$
	Twist distribution	$\varepsilon_1, \varepsilon_5, \varepsilon_8, \varepsilon_9, \varepsilon_{15}$
	Relative thickness distribution	$(t/c)_1, (t/c)_5, (t/c)_9, (t/c)_{14}$
	Inboard rear spar position	x_{RS}/c
	Control surface deflection angles	$\delta_{in}, \delta_{out}, \delta_{ail}$
Constraints	Maximum take-off mass	$m_{MTO} = 245\,000\text{ kg}$
	Maximum payload	$m_{P,max} = 48\,000\text{ kg}$
	Residual mass ratio	$m_{Res}/m_{MTO} = 0.3763$
	Specific mass of leading edge high lift device	$m_{LE}/S_{LE} = 30\text{ kg/m}^2$
	Specific mass of trailing edge high lift device	$m_{TE}/S_{TE} = 50\text{ kg/m}^2$
	Thrust specific fuel consumption	$TSFC = \frac{0.245\text{ h}^{-1} + 0.415\text{ h}^{-1} Ma}{g} \sqrt{\frac{\Theta}{\Theta_{SL}}}$
	Wingspan (FAA Group V/ICAO Code E)	$52\text{ m} \leq b \leq 65\text{ m}$
	Rib spacing	$\Delta s_{Ri} = 0.75\text{ m}$
	Fuel tank volume	$V_F \geq V_{F,req}$
	Outer main gear wheel span (ICAO Code E)	$9\text{ m} \leq 2 y_{MG} \leq 14\text{ m}$
	Nose gear static load ratio	$5\% \leq F_{NG}/m g \leq 20\%$
	Tip back angle	$\tau_{tb} \geq 15^\circ$
	Overturn angle	$\tau_{ot} \leq 63^\circ$
	Take-off rotation angle	$\alpha_{TO} \leq 9^\circ$
	Clearance of tail, engine, and wing	$h_{TC}, h_{EC}, h_{WC} \geq 0.4\text{ m}$
	Nose down engine clearance	$h_{NDEC} \geq 0.2\text{ m}$
	Relative x-position of main gear wheel on ground	$x_{MG}/c_{MAC} = 0.6$
	Castor angle of main gear leg	$80^\circ \leq \tau_{Cas} \leq 90^\circ$
	Distance between main gear and center wing box	$2.0\text{ m} \leq \Delta s_{MG/CWB} \leq 2.4\text{ m}$
	Distance between main gear and symmetry plane	$1.4\text{ m} \leq \Delta s_{MG/Sym} \leq 1.6\text{ m}$
Distance between main gear and rear spar	$0.6\text{ m} \leq \Delta s_{MG/RS} \leq 1.4\text{ m}$	
Distance between flap and support beam	$\Delta s_{Flap/SB} \geq 0.2\text{ m}$	
Distance between flap and rear spar	$\Delta s_{Flap/RS} \geq 0.065 c_{MAC}$	
Distance between aileron and rear spar	$\Delta s_{Ail/RS} \geq 0.04 c_{MAC}$	

TAB 5. Design parameters and constraints.

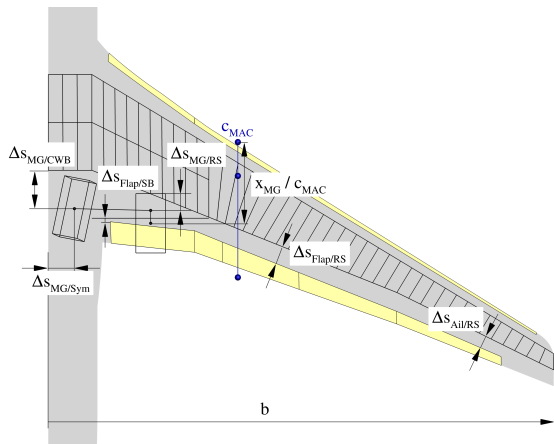


FIG 6. Geometrical constraints.

For each aircraft category the outer main gear wheel span has to be within the given limits. Furthermore, the geometrical constraints for nose down engine clearance h_{NDEC} , touch down tail clearance h_{TC} , and engine and wing clearances h_{EC}, h_{WC} for a bank

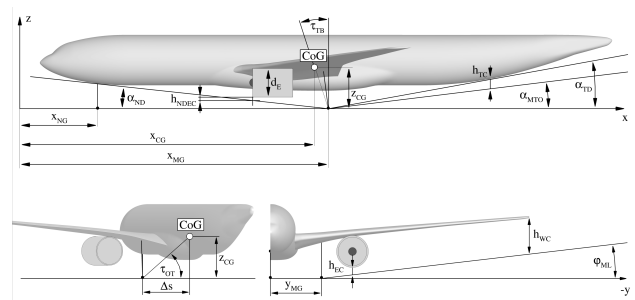


FIG 7. Landing gear constraints.

angle of $\varphi = 5^\circ$ have to be fulfilled. The selected values are given in TAB. 5.

The introduced landing gear integration consists of a design loop for automatic main gear positioning. Thereby, the main gear wing attachment point is shifted from inboard to outboard position and from front to rear position for each span location. All geometrical constraints are checked for each prescribed position, until a feasible design is found.

In TAB. 5 the introduced design parameters and constraints are summarized. The design parameters include wing planform and wing section parameters. In addition the inboard rear spar position has been used as design parameter. The control surface deflection angles have been introduced for the wing optimizations with active maneuver load alleviation. The constraints consist of mass constraints, propulsion constraints, geometrical constraints for airport conformity, landing gear and control surface integration constraints, flight mission constraints, and structural sizing constraints. In TAB. 5 the used values and their limits are given.

3.2. Wing optimization results without MLA

In this section the wing optimization results without the consideration of active maneuver load alleviation are presented. The selected global design parameters of the wing optimizations are summarized in TAB. 6. Based on the Airbus XRF1 reference aircraft geometry, the twist and thickness distribution have been optimized with the result representing the baseline. In the next step the wing planform including the twist and thickness distribution have been optimized. The last optimization additionally considers the structural concept of a more flexible wing by changing the structural concept and the maximum strain allowable. The resulting wing geometries and the corresponding twist and thickness distributions are shown in FIG. 8. Thereby, the wing planform, the wing box geometry with the spars and ribs, the landing gear including the support beam, and the control surface geometries are presented. The twist distribution for the rigid "jig-shape" and the elastic "flight-shape" are shown for the optimized wings. The shown "flight-shape" results from the wing deformations at the beginning of the "study mission" (see TAB. 2). For the structural interpretation of the results the absolute wing thickness distribution is given. In addition, the relative thickness distribution for the aerodynamic interpretation is presented.

The result of the twist and thickness optimization shows a wing with a significant thin inboard wing section. With the aero-structural wing optimization an optimal trade-off between cruise flight performance and wing mass in terms of combined fuel consumption has been achieved. In TAB. 7 an overview of all relevant values is given. A value lower than one of the used fuel tank volume for the design mission indicates that the fuel volume constraint is fulfilled. The results of the wing planform optimizations show increased wingspan and reduced taper ratio. This leads to increased cruise flight performance without drawbacks due to wing mass changes.

Based on the significant mass reduction of the more flexible wing concept the wing optimization leads to an optimized wing design with further increased wingspan and further decreased relative airfoil thicknesses in the inboard wing region. The corresponding cruise flight performance in terms of lift-to-drag ratios

is increased and the wing mass is reduced. In comparison to the wing with conventional wing structure the more flexible wing shows a fuel consumption reduction in the order of 3 %.

In FIG. 9 an overview of the aerodynamic results is given for the optimized wings. For each lift distribution the related elliptical lift distribution is shown by a dashed line and the corresponding center of lift is indicated by a grey rectangle as a reference. The elliptical lift distribution is optimum for planar wings in terms of lift induced drag. For the cruise flight condition the result of the twist and thickness optimization shows a nearly elliptical lift distribution. The results of the wing planform optimizations show cruise flight lift distributions with increased inboard loading in comparison to the elliptical lift distribution. The corresponding center of lift is indicated by a black circle. This leads in combination with the relative airfoil thickness to higher values for the isentropic Mach number in the inboard wing region. In the pull up maneuver a significant inboard load shift occurs due to static aeroelastic effects of the backward swept wing [49, 50]. This inboard load shift is stronger for the more flexible wing in comparison to the optimized wings with conventional wing structure. Thereby, the inboard load shift is related to a forward shifting of the center of pressure in the case of backward swept wings and the aircraft trimming redistributes the lift between the wing and the horizontal tail. As a result, the lift of the horizontal tail increases and simultaneously the lift of the wing decreases.

The resulting wing deformations are presented for the cruise flight condition and the 2.5g symmetric pull up maneuver in comparison to the rigid jig-shape. The more flexible wing shows higher deflections due to the modified structural concept and the increased strain allowable.

In addition an overview of the structural results is presented in FIG. 9. The element thicknesses (sum of skin thickness and stringer height) are shown for the spars, ribs, and covers of the sized wing box.

All optimized wings with the conventional wing box structure show a similar thickness distribution. The upper and lower covers have the highest and the biggest thicknesses of all components. Therefore, the covers have the biggest mass contribution. All optimization results show a thickness peak at the engine position and the kink.

In the case of the more flexible wing with the increased maximum strain allowable the mass of the upper and lower covers decreases significantly, because the maximum strain criteria is the dominant criteria for the covers on the conventional wing structure. Furthermore, the spars of the more flexible wing are getting thinner due to the reduced airfoil thickness and the corresponding reduction of buckling areas, where stability is still the sizing criteria for the spars. While optimizing the airfoil thickness the thicknesses of the covers increase slightly with decreasing airfoil thicknesses.

		Twist and thickness optimization (Baseline)	Planform, twist, and thickness optimization	More flexible wing optimization
Wing area	S	-	1	1
Aspect ratio	A	-	1	1
Taper ratios	$\lambda_{5/2}, \lambda_{9/5}, \lambda_{14/9}$	-	3	3
Leading edge sweep angle	φ_{LE}	-	1	1
Twist distribution	$\varepsilon_1, \varepsilon_5, \varepsilon_8, \varepsilon_9, \varepsilon_{15}$	5	5	5
Airfoil thickness distribution	$(t/c)_1, (t/c)_5, (t/c)_9, (t/c)_{14}$	4	4	4
Control surface extension	$\Delta(c_F/c)$	-	1	1
Inboard rear spar position	x_{RS}/c	-	1	1
Control surface deflections	$\delta_{in,LC1}, \delta_{out,LC1}, \delta_{ail,LC1}$ $\delta_{in,LC2}, \delta_{out,LC2}, \delta_{ail,LC2}$	-	-	-
Global design parameters	n_{DP}	9	17	17

TAB 6. Global design parameters of wing optimizations without maneuver load alleviation.

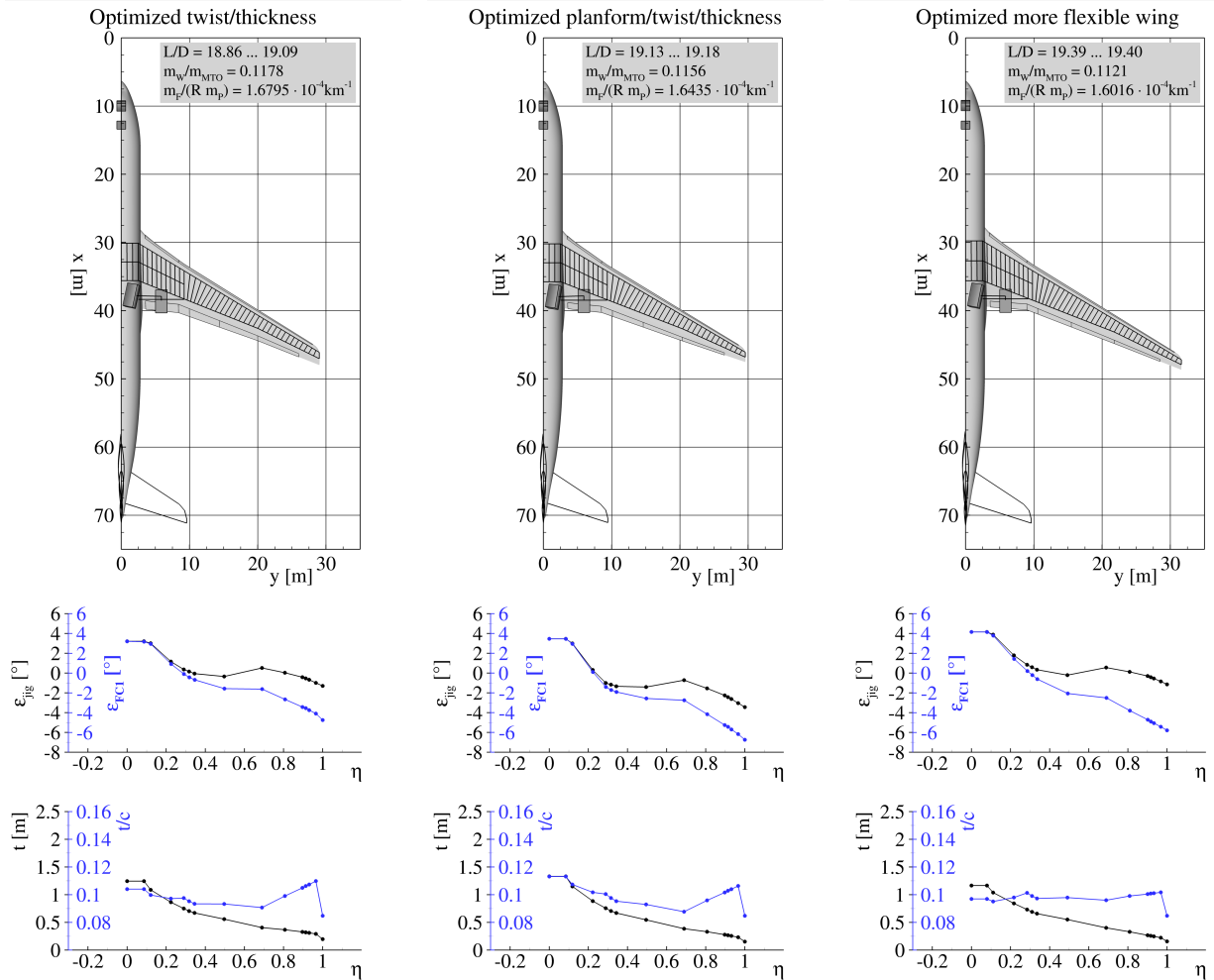


FIG 8. Geometry overview of wing optimizations without maneuver load alleviation.

			Optimized twist and thickness (Baseline)	Optimized planform, twist, and thickness	Optimized more flexible wing
Wing Geometry	Wing area	S_W	376.2 m ²	371.1 m ²	387.4 m ²
	Wingspan	b_W	58.01 m	59.15 m	63.20 m
	Mean aerodynamic chord	$c_{W,MAC}$	7.76 m	7.61 m	7.56 m
	Aspect ratio	A_W	8.946	9.428	10.309
	Taper ratio	λ_W	0.195	0.153	0.154
	Leading edge sweep angle	$\varphi_{W,LE}$	31.9°	31.3°	31.6°
	Flap spar offset	$\Delta s_{Flap/RS}$	0.99 m	1.14 m	0.84 m
	Aileron spar offset	$\Delta s_{Ail/RS}$	0.64 m	0.67 m	0.64 m
	Useable fuel tank volume	V_F	108.4 m ³	112.7 m ³	113.3 m ³
Tail geometry	Horizontal tail area	S_{HTP}	69.2 m ²	67.0 m ²	69.4 m ²
	Vertical tail area	S_{VTP}	49.9 m ²	50.2 m ²	56.0 m ²
Landing Gear	Outer main gear wheel span	$2y_{MG}$	11.74 m	11.86 m	11.67 m
	Nose gear static load factor	$F_{NG}/(m g)$	0.060 ... 0.084	0.059 ... 0.083	0.059 ... 0.082
	Tipback angle	τ_{TB}	18.6° ... 25.7°	18.3° ... 25.4°	17.9° ... 24.8°
	Overturn angle	τ_{OT}	40.6° ... 40.7°	40.2° ... 40.3°	41.1° ... 41.2°
	Tail down angle	α_{TD}	11.0°	11.0°	11.2°
	Main gear spar offset	$\Delta s_{MG/RS}$	0.95 m	0.75 m	0.95 m
	Main gear flap offset	$\Delta s_{Flap/SB}$	0.20 m	0.35 m	0.32 m
Masses	Mass of covers	$m_{W,covers}$	14 223 kg	13 898 kg	13 267 kg
	Mass of spars	$m_{W,spars}$	2917 kg	2954 kg	2355 kg
	Mass of ribs	$m_{W,ribs}$	2501 kg	2572 kg	2915 kg
	Wing box mass	$m_{W,box}$	19 640 kg	19 424 kg	18 537 kg
	Wing mass ratio	m_W/m_{MTO}	0.1178	0.1156	0.1121
	Operational empty mass ratio	m_{OE}/m_{MTO}	0.5199	0.5174	0.5149
Maneuver n=2.5	Lift-to-drag ratio	L/D	12.40	12.89	12.73
	Center of pressure	$2 y_{CoP}/b$	0.371	0.362	0.353
Study mission	Lift-to-drag ratio	L/D	18.86	19.13	19.40
	Center of pressure	$2 y_{CoP}/b$	0.420	0.399	0.387
	Fuel consumption	$m_F/(R m_P)$	$1.566 \times 10^{-4} \text{ km}^{-1}$	$1.537 \times 10^{-4} \text{ km}^{-1}$	$1.510 \times 10^{-4} \text{ km}^{-1}$
High speed mission	Lift-to-drag ratio	L/D	17.95	18.05	18.10
	Center of pressure	$2 y_{CoP}/b$	0.415	0.392	0.379
	Fuel consumption	$m_F/(R m_P)$	$1.631 \times 10^{-4} \text{ km}^{-1}$	$1.616 \times 10^{-4} \text{ km}^{-1}$	$1.606 \times 10^{-4} \text{ km}^{-1}$
Design mission	Payload	m_P	33 278 kg	34 185 kg	35 463 kg
	Used fuel tank volume ratio	$V_{F,req}/V_F$	0.973	0.932	0.920
	Lift-to-drag ratio	L/D	19.09	19.18	19.39
	Center of pressure	$2 y_{CoP}/b$	0.413	0.392	0.377
	Fuel consumption	$m_F/(R m_P)$	$1.923 \times 10^{-4} \text{ km}^{-1}$	$1.865 \times 10^{-4} \text{ km}^{-1}$	$1.784 \times 10^{-4} \text{ km}^{-1}$
Objective	Combined fuel consumption	$m_F/(R m_P)$	$1.680 \times 10^{-4} \text{ km}^{-1}$	$1.644 \times 10^{-4} \text{ km}^{-1}$	$1.602 \times 10^{-4} \text{ km}^{-1}$

TAB 7. Results overview of wing optimizations without maneuver load alleviation.

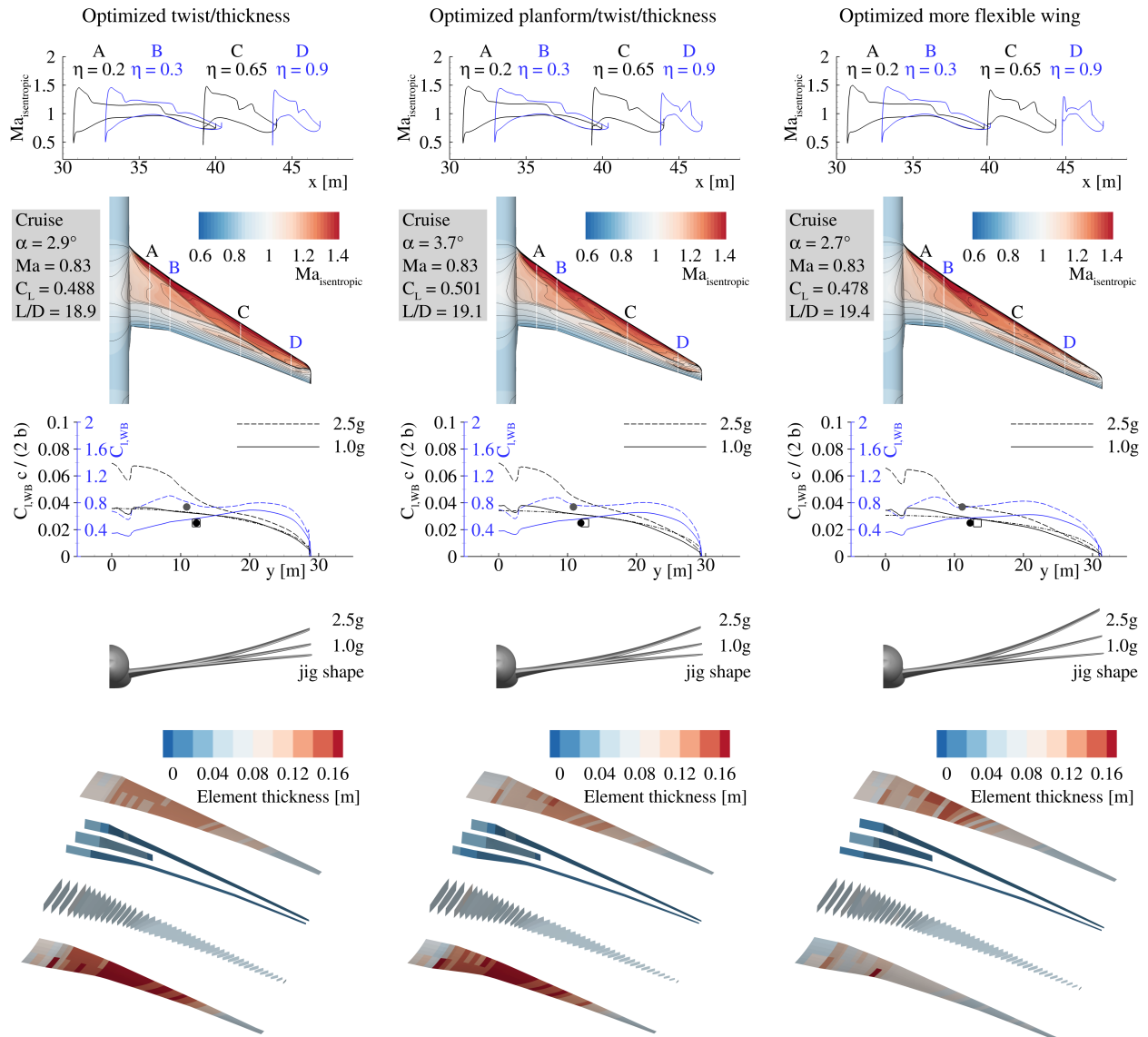


FIG 9. Aerodynamic and structural results overview of wing optimizations without maneuver load alleviation.

3.3. Wing optimization results with MLA

In this section the wing optimization results with the consideration of active maneuver load alleviation are presented. The selected global design parameters of the wing optimizations are summarized in TAB. 8. Based on the Airbus XRF1 reference aircraft geometry, the twist and thickness distribution and the inboard and outboard control surface deflections have been optimized and the result is representing the baseline with active maneuver load alleviation. In the next optimization the wing planform including the twist and thickness distribution have been optimized. The last optimization additionally considers the structural concept of a more flexible wing by changing the structural concept and the maximum strain allowable. The resulting wing geometries and the corresponding twist and thickness distributions are shown in FIG. 10 for the wing optimizations with active maneuver load alleviation. As a comparison to the results of the wing optimizations without consideration of active maneuver load alleviation, the outer shape and inner wing structure are presented for the wings with active maneuver load alleviation.

The results show very thin inboard wing sections for the wing with optimized twist and thickness distribution and the optimized more flexible wing. Based on the significant mass reduction due to the active maneuver load alleviation system, the aero-structural wing optimizations lead to wings with decreased relative airfoil thicknesses in the inboard wing region. In TAB. 9 an overview of all relevant values is given. The wing mass of the baseline without maneuver load alleviation has been reduced in the order of 2.2t in comparison to the twist and thickness optimized wing with active load alleviation. The results of the wing planform optimizations show increased wingspan and reduced taper ratio here again. This leads to increased cruise flight performance without drawbacks due to wing mass changes. In comparison to the wings without maneuver load alleviation the optimization results with consideration of with active maneuver load alleviation show wing geometries with increased wingspan and aspect ratio, decreased taper ratio and improved cruise flight performance in terms of lift-to-drag ratios. The corresponding fuel consumptions have been reduced due to improved cruise flight performance without drawbacks due to operational empty mass changes. Furthermore, the wing optimizations with active maneuver load alleviation result in more inboard center of pressure positions for maneuver flight and similar center of pressure positions under cruise flight conditions. This larger inboard load shift is the result of the control surface deflections given in TAB. 9 and the reduced wing stiffness. All optimized wings with active maneuver load alleviation fulfill the fuel volume constraint.

An overview of the aerodynamic results is given in FIG. 11 for the optimized wings with active maneuver load alleviation in comparison to the optimization results of the wings without the consideration of

active maneuver load alleviation. The resulting wing deformations are presented for the cruise flight condition and the $2.5g$ symmetric pull up maneuver in comparison to the rigid jig-shape. The wings with active maneuver load alleviation show reduced deflections for the pull up maneuver and higher deflections under cruise flight conditions due to reduced wing stiffness. Furthermore, the more flexible wing show higher deflections due to the modified structural concept and the increased strain allowable. The results of the wing planform optimizations show cruise flight lift distributions with increased inboard loading in comparison to the elliptical lift distribution. In the pull up maneuver a significant inboard load shift occurs due to active control surface deflections and static aeroelastic effects of the backward swept wing. This inboard load shift of the optimized wings with active maneuver load alleviation is larger in comparison to the optimized wings without the active load alleviation system. As expected, the inboard load shift increases further for the more flexible wing. The wing planform optimization of the more flexible wing with active maneuver load alleviation shows a strong reduction of wing bending in the pull up maneuver. Thereby, the inboard load shift is related to a forward shifting of the center of pressure in the case of backward swept wings and the aircraft trimming redistributes the lift between the wing and the horizontal tail. As a result, the lift of the horizontal tail increases and simultaneously the lift of the wing decreases.

In analogy to the results without maneuver load alleviation an overview of the structural results for the wings with an active maneuver load alleviation system is presented in FIG. 11. With the reduced level of aerodynamic loads the mass of the upper and lower covers decreases significantly. In the case of the planform, twist, and thickness optimization a similar load level is obtained for an increased wingspan by introducing the active maneuver load alleviation system. Furthermore, the spars are getting thinner due to the reduced airfoil thickness and the corresponding reduction of buckling areas, where stability is still the sizing criteria for the spars. While optimizing the airfoil thickness the thicknesses of the covers increase slightly with decreasing airfoil thicknesses. By introducing the more flexible wing concept, the increased maximum strain allowable leads again to reduced thicknesses of the wing box structure.

		Twist and thickness optimization with MLA	Planform, twist, and thickness optimization with MLA	More flexible wing optimization with MLA
Wing area	S	-	1	1
Aspect ratio	A	-	1	1
Taper ratios	$\lambda_{5/2}, \lambda_{9/5}, \lambda_{14/9}$	-	3	3
Leading edge sweep angle	φ_{LE}	-	1	1
Twist distribution	$\varepsilon_1, \varepsilon_5, \varepsilon_8, \varepsilon_9, \varepsilon_{15}$	5	5	5
Airfoil thickness distribution	$(t/c)_1, (t/c)_5, (t/c)_9, (t/c)_{14}$	4	4	4
Control surface extension	$\Delta(c_F/c)$	-	1	1
Inboard rear spar position	x_{RS}/c	-	1	1
Control surface deflections	$\delta_{in,LC1}, \delta_{out,LC1}, \delta_{ail,LC1}$	3	3	3
	$\delta_{in,LC2}, \delta_{out,LC2}, \delta_{ail,LC2}$	3	3	3
Global design parameters	n_{DP}	15	23	23

TAB 8. Global design parameters for wing optimizations with active maneuver load alleviation.

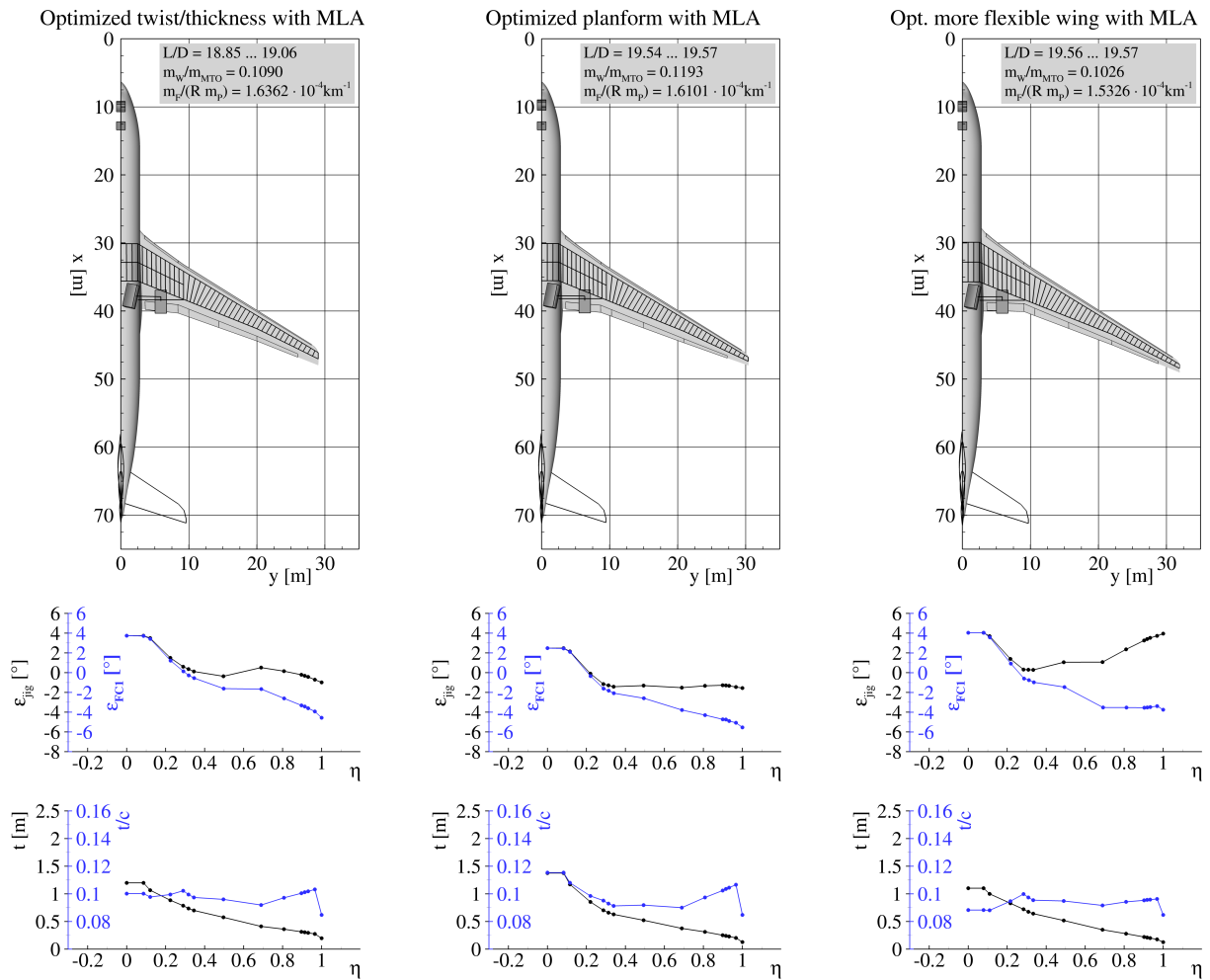


FIG 10. Geometry overview of wing optimizations with active maneuver load alleviation.

			Optimized twist and thickness with MLA	Optimized planform, twist, and thickness with MLA	Optimized more flexible wing with MLA
Wing Geometry	Wing area	S_W	376.2 m ²	372.0 m ²	384.5 m ²
	Wingspan	b_W	58.01 m	60.70 m	63.79 m
	Mean aerodynamic chord	$c_{W,MAC}$	7.76 m	7.62 m	7.76 m
	Aspect ratio	A_W	8.946	9.904	10.582
	Taper ratio	λ_W	0.195	0.128	0.120
	Leading edge sweep angle	$\varphi_{W,LE}$	31.9°	31.8°	32.3°
	Flap spar offset	$\Delta s_{Flap/RS}$	0.99 m	0.99 m	0.59 m
	Aileron spar offset	$\Delta s_{Ail/RS}$	0.64 m	0.55 m	0.45 m
	Useable fuel tank volume	V_F	108.5 m ³	110.9 m ³	106.8 m ³
Tail geometry	Horizontal tail area	S_{HTP}	69.2 m ²	67.2 m ²	70.7 m ²
	Vertical tail area	S_{VTP}	49.9 m ²	51.6 m ²	56.0 m ²
Landing Gear	Outer main gear wheel span	$2 y_{MG}$	11.75 m	12.66 m	11.70 m
	Nose gear static load factor	$F_{NG}/(m g)$	0.060 ... 0.084	0.059 ... 0.083	0.060 ... 0.084
	Tipback angle	τ_{TB}	18.5° ... 25.6°	17.4° ... 24.1°	18.5° ... 25.5°
	Overturn angle	τ_{OT}	40.8° ... 40.9°	40.1° ... 40.3°	40.9° ... 41.1°
	Tail down angle	α_{TD}	11.1°	11.6°	11.1°
	Main gear spar offset	$\Delta s_{MG/RS}$	0.95 m	0.70 m	0.85 m
	Main gear flap offset	$\Delta s_{Flap/SB}$	0.20 m	0.48 m	0.31 m
Masses	Mass of covers	$m_{W,covers}$	12 314 kg	14 879 kg	10 995 kg
	Mass of spars	$m_{W,spars}$	2829 kg	2865 kg	2232 kg
	Mass of ribs	$m_{W,ribs}$	2335 kg	2513 kg	3021 kg
	Wing box mass	$m_{W,box}$	17 478 kg	20 256 kg	16 247 kg
	Wing mass ratio	m_W/m_{MTO}	0.1090	0.1193	0.1026
	Operational empty mass ratio	m_{OE}/m_{MTO}	0.5110	0.5213	0.5056
Maneuver n=2.5	Lift-to-drag ratio	L/D	14.61	14.26	12.87
	Center of pressure	$2 y_{CoP}/b$	0.328	0.332	0.292
	Inboard flap deflection	δ_{in}	15.8°	10.5°	16.4°
	Outboard flap deflection	δ_{out}	-11.3°	-7.8°	-19.9°
	Aileron deflection	δ_{ail}	-16.2°	-9.2°	-20.0°
Study mission	Lift-to-drag ratio	L/D	18.85	19.54	19.57
	Center of pressure	$2 y_{CoP}/b$	0.416	0.401	0.391
	Fuel consumption	$m_F/(R m_P)$	$1.547 \times 10^{-4} \text{ km}^{-1}$	$1.513 \times 10^{-4} \text{ km}^{-1}$	$1.476 \times 10^{-4} \text{ km}^{-1}$
High speed mission	Lift-to-drag ratio	L/D	17.66	18.67	18.49
	Center of pressure	$2 y_{CoP}/b$	0.410	0.394	0.383
	Fuel consumption	$m_F/(R m_P)$	$1.638 \times 10^{-4} \text{ km}^{-1}$	$1.570 \times 10^{-4} \text{ km}^{-1}$	$1.549 \times 10^{-4} \text{ km}^{-1}$
Design mission	Payload	m_P	35 315 kg	34 519 kg	38 304 kg
	Used fuel tank volume ratio	$V_{F,req}/V_F$	0.973	0.933	0.969
	Lift-to-drag ratio	L/D	19.06	19.57	19.56
	Center of pressure	$2 y_{CoP}/b$	0.408	0.393	0.379
	Fuel consumption	$m_F/(R m_P)$	$1.815 \times 10^{-4} \text{ km}^{-1}$	$1.819 \times 10^{-4} \text{ km}^{-1}$	$1.640 \times 10^{-4} \text{ km}^{-1}$
Objective	Combined fuel consumption	$m_F/(R m_P)$	$1.636 \times 10^{-4} \text{ km}^{-1}$	$1.610 \times 10^{-4} \text{ km}^{-1}$	$1.533 \times 10^{-4} \text{ km}^{-1}$

TAB 9. Results overview of wing optimizations with active maneuver load alleviation.

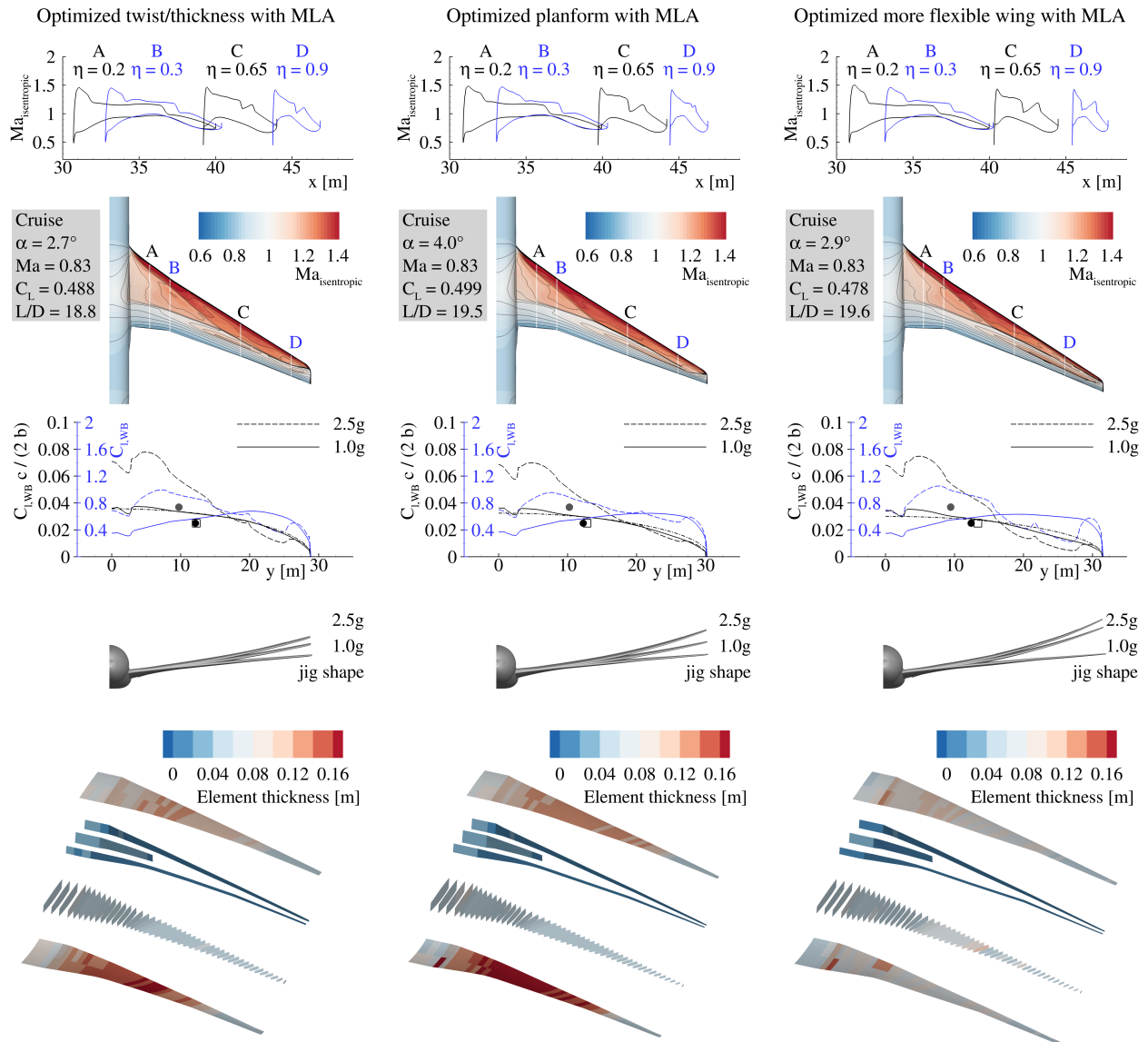


FIG 11. Aerodynamic and structural results overview of wing optimizations with active maneuver load alleviation.

Optimization	Reference	Reduction of combined fuel consumption
Baseline with MLA	Optimized twist and thickness (Baseline)	2.6 %
Optimized planform, twist, and thickness with MLA	Optimized planform, twist, and thickness	2.0 %
Optimized more flexible wing with MLA	Optimized more flexible wing	4.3 %
Optimized more flexible wing with MLA	Airbus XRF1 (optimized twist, results not shown)	12.9 %

TAB 10. More flexible wing optimization results overview.

3.4. Result overview and assessment of active maneuver load alleviation

The main results of the aero-structural wing optimizations are summarized in TAB. 10. The percentage of reduction in combined fuel consumption is presented in the last row and shows the potential of active maneuver load alleviation to reduce the CO_2 emissions per passenger kilometer.

With the introduced active maneuver load alleviation a reduction of the combined fuel consumption between 2% and 3% has been achieved for the optimizations with conventional composite wing box structure. The active maneuver load alleviation shows for wing optimizations with the more flexible wing concept an additional reduction of the combined fuel consumption in the order of 2% due to snowball effects. In comparison to the twist optimized reference aircraft Airbus XRF1, the introduction of the active maneuver load alleviation technology and of the more flexible wing concept, leads to reductions of the combined fuel consumption in the order of 13% after aero-structural wing optimization. The results for the reference aircraft Airbus XRF1 are not presented here, because of restricted publication rules.

In FIG. 12 an overview for the results of the aero-structural wing optimizations is shown. For all aero-structural wing analysis the cruise flight performance, the wing mass ratio, and the corresponding combined fuel consumption are summarized.

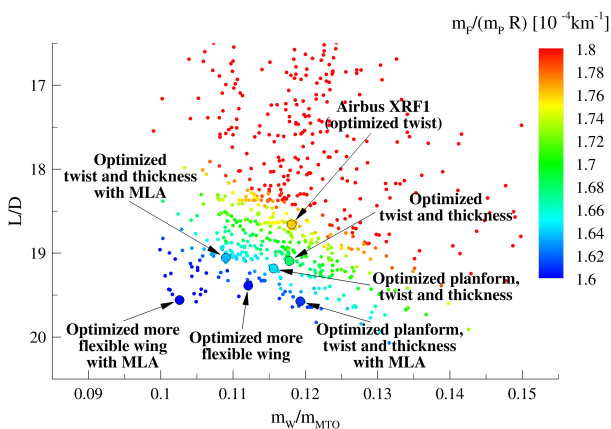


FIG 12. Wing optimization results overview.

The combined fuel consumption depends on cruise flight performance and wing mass. The global search

in the design space shows different combinations of these two counterparts with the same objective function value. However, the global search has been converged with a acceptable accuracy for practical wing design and optimization.

4. CONCLUSION AND OUTLOOK

In this work, the assessment of the active maneuver load alleviation has been successfully demonstrated by using an integrated process for aero-structural wing optimization based on high fidelity simulation methods. The comparison of optimization results with the same objective function, design parameters, and constraints allows a proper technology assessment. To find the optimum trade-off between aerodynamic performance and wing mass, the twist and thickness distribution and the wing planform design parameters have been involved in the wing optimization. The results of this optimization show the expected reduction of the combined fuel consumption due to decreased wing mass based on active adaptation of the load distribution in maneuver flight and an increased aerodynamic performance under cruise flight conditions. This increase in aerodynamic performance has been achieved with higher aspect ratio and reduced taper ratio of the wing.

With the application of active maneuver load alleviation, the significance of the aerodynamic limits of control surface deflections due to flow separations for the prediction of maneuver loads has been shown. The structural wing sizing based on a reduced level of aerodynamic loads, results in a significant wing mass reduction and more wing flexibility.

Within the wing planform optimizations only 1% of the wing geometries in the selected design space have fulfilled the geometrical constraints and have been considered in the aero-structural wing analysis. This observation shows the importance of the consideration of landing gear integration and control surface constraints.

Another aspect of the wing optimization results obtained, is the resulting thin inboard wing, which contradicts conceptual design estimations based on handbook methods and is significantly lower than the values of current aircraft designs. One reason for this is the requested flexibility of airlines for extended range missions, which requires additional fuel tank volume.

In the future, the processes for wing optimization have to be extended with engine design and integration, gust loads prediction, and take-off and landing constraints. Furthermore, the airfoil design has to be integrated with the usage of an airfoil catalog or by gradient based shape optimization. With increasing computational resources and progress in numerical processes, based in high fidelity methods, it is possible for more disciplines and there interactions to be considered in the assessment of new aircraft technologies and configurations.

ACKNOWLEDGMENTS

The authors would like to thank Airbus for providing the XRF1 research test case as opportunity for demonstrating the approaches presented in this publication.

Contact address:

tobias.wunderlich@dlr.de

References

- [1] European Commission. *2008 Addendum to the Strategic Research Agenda*. Luxembourg, Belgium: Office for Official Publications of the European Communities, 2008.
- [2] European Commission. *Flightpath 2050 Europe's Vision for Aviation*. Luxembourg, Belgium: Office for Official Publications of the European Communities, 2011.
- [3] F. Collier et al. "Environmentally Responsible Aviation-Real Solutions for Environmental Challenges Facing Aviation". In: *27th Interantional Congress of the Aeronautical Sciences, ICAS 2010, Nice, France*. ICAS Conference Paper. Sept. 2010.
- [4] G. M. Bezos-O'Connor et al. "Fuel Efficiencies Through Airframe Improvements". In: *3rd AIAA Atmospheric Space Environments Conference*. AIAA 2011-3530. June 2011.
- [5] G. W. K. Kenway and J. R. R. A. Martins. "High-fidelity aerostructural optimization considering buffet onset". In: *Proceedings of the 16th AIAA/ISSMO Multidisciplinary Analysis and Optimization Conference, Texas, USA*. June 2015.
- [6] R. J. White. "Improving the Airplane Efficiency by Use of Wing Maneuver Load Alleviation". In: *Journal of Aircraft* 8.10 (1971), pp. 769–775.
- [7] G. E. Bendixen et al. "Digital active control system for load alleviation for the Lockheed L-1011". In: *The Aeronautical Journal* 85.849 (1981), pp. 430–436.
- [8] A. Jameson et al. "Multi-point Aero-Structural Optimization of Wings Including Planform Variations". In: *45th Aerospace Sciences Meeting and Exhibit, Reno, Nevada, USA*. AIAA 2007-764. 2007.
- [9] J. R. R. A. Martins and J. T. Hwang. "Review and Unification of Methods for Computing Derivatives of Multidisciplinary Computational Models". In: *AIAA Journal* 51 (2013), pp. 2582–2599.
- [10] R. P. Liem et al. "Multimission Aircraft Fuel-Burn Minimization via Multipoint Aerostructural Optimization". In: *AIAA Journal* 53 (2015), pp. 104–122.
- [11] S. Keye et al. "Aero-Structural Optimization of the NASA Common Research Model". In: *AIAA Aviation and Aeronautics Forum and Exposition (AVIATION)*. AIAA 2017-4145. June 2017.
- [12] M. Abu-Zurayk et al. "Sensitivity-based Multifidelity Multidisciplinary Optimization of a Powered Aircraft Subject to a Comprehensive Set of Loads". In: *AIAA Aviation Forum 2020*. June 2020.
- [13] S. Görtz et al. "Multi-Level MDO of a Long-Range Transport Aircraft Using a Distributed Analysis Framework". In: *18th AIAA/ISSMO Multidisciplinary Analysis and Optimization Conference, Denver, USA*. June 2017.
- [14] S. Görtz et al. "DLR-Projekt VicToria - Virtual Aircraft Technology Integration Platform". In: *Deutscher Luft- und Raumfahrtkongress 2018*. Sept. 2018.
- [15] S. Görtz et al. "Overview of Collaborative Multi-Fidelity Multidisciplinary Design Optimization Activities in the DLR Project VicToria". In: *AIAA Aviation Forum 2020*. June 2020.
- [16] T. F. Wunderlich et al. "Overview of collaborative high performance computing-based MDO of transport aircraft in the DLR project VicToria". In: *Deutscher Luft- und Raumfahrtkongress 2018*. Sept. 2018.
- [17] C. Ilic et al. "Cybermatrix protocol: a novel approach to highly collaborative and computationally intensive multidisciplinary aircraft optimization". In: *AIAA Aviation Forum 2020*. June 2020.
- [18] T. F. Wunderlich et al. "Multidisciplinary optimization of an NLF forward swept wing in combination with aeroelastic tailoring using CFRP". In: *CEAS Aeronautical Journal* 8.4 (2017), pp. 673–690.
- [19] T. F. Wunderlich and L. Reimer. "Integrated Process Chain for Aerostructural Wing Optimization and Application to an NLF Forward Swept Composite Wing". In: *AeroStruct: Enable and Learn How to Integrate Flexibility in Design*. Ed. by R. Heinrich. Vol. 138. Notes on Numerical Fluid Mechanics and Multidisciplinary Design (NNFM). Springer, Cham, 2018, pp. 3–33.
- [20] J. R. R. A. Martins and A. B. Lambe. "Multidisciplinary Design Optimization: A Survey of Architectures". In: *AIAA Journal* 51 (2013), pp. 2049–2075.
- [21] T. F. Wunderlich et al. "Global Aero-Structural Design Optimization of More Flexible Wings for Commercial Aircraft". In: *AIAA Aviation Forum 2020*. June 2020.
- [22] A. B. Lambe and J. R. R. A. Martins. "Extensions to the Design Structure Matrix for the Description of Multidisciplinary Design Analysis and Optimization Processes". In: *Structural and Multidisciplinary Optimization* 46 (2012), pp. 273–284.
- [23] C. M. Liersch and M. Hepperle. "A distributed toolbox for multidisciplinary preliminary aircraft design". In: *CEAS Aeronautical Journal* 2.1–4 (2011), pp. 57–68.
- [24] B. Nagel et al. "Communication in Aircraft Design Can we Establish a Common Language". In: *28th Interantional Congress of the Aeronautical Sciences, ICAS 2012*. ICAS Conference Paper. Sept. 2012.

- [25] A. Rempke. "Netzdeformation mit Elastizitätsanalogie in multidisziplinärer FlowSimulator-Umgebung". In: *20. DGLR - Fach - Symposium der STAB 2016*. Vol. 2016. 2016, pp. 128–129.
- [26] M. Meinel and G. O. Einarsson. "The FlowSimulator framework for massively parallel CFD applications". In: *PARA 2010 conference, 6-9 June, Reykjavik, Iceland*. 2010.
- [27] L. Reimer et al. "Multidisciplinary Analysis Workflow with the FlowSimulator". In: *Proceedings of the Onera Scientific Day 2012—CFD Workflow: Mesh, Solving, Visualizing, ...* Ed. by C. Benoit et al. Vol. 19. Amphithéâtre Becquerel, École Polytechnique, Palaiseau, 2012, pp. 23–30.
- [28] L. Reimer et al. "Towards Higher-Precision Maneuver and Gust Loads Computations of Aircraft: Status of Related Features in the CFD-Based Multidisciplinary Simulation Environment FlowSimulator". In: *New Results in Numerical and Experimental Fluid Mechanics XII*. Ed. by A. Dillmann et al. Cham: Springer International Publishing, 2020, pp. 597–607.
- [29] T. Führer et al. "Automated model generation and sizing of aircraft structures". In: *Aircraft Engineering and Aerospace Technology* 88.2 (2016), pp. 268–276.
- [30] C. Geuzaine and J.-F. Remacle. "Gmsh: A 3-D finite element mesh generator with built-in pre- and post-processing facilities". In: *International Journal for Numerical Methods in Engineering* 79.11 (2009), pp. 1309–1331.
- [31] R. Kamakoti and W. Shyy. "Fluid-structure interaction for aeroelastic applications". In: *Progress in Aerospace Sciences* 40.8 (2005), pp. 535–558.
- [32] X. B. Lam et al. "Coupled Aerostructural Design Optimization Using the Kriging Model and Integrated Multiobjective Optimization Algorithm". In: *Journal of Optimization Theory and Applications* 142.3 (2009), pp. 533–556.
- [33] T. Gerhold. "Overview of the Hybrid RANS TAU-Code, In: Kroll N., Fassbender J. (Eds) MEGAFLOW - Numerical Flow Simulation Tool for Transport Aircraft Design". In: *Notes on Multidisciplinary Design* 89 (2005).
- [34] D. Schwamborn et al. "The DLR TAU-Code: Recent Applications in Research and Industry". In: *European Conference on Computational Fluid Dynamics, EC-COMAS CFD 2006 Conference, Delft, The Netherlands*. 2006.
- [35] E. N. Tinoco et al. "Summary Data from the Sixth AIAA CFD Drag Prediction Workshop: CRM Cases". In: *Journal of Aircraft* 55.4 (2018), pp. 1352–1379.
- [36] S. Dähne et al. "Steps to Feasibility for Laminar Wing Design in a Multidisciplinary Environment". In: *29th Congress of the International Council of the Aeronautical Sciences, ICAS 2014*. Sept. 2014.
- [37] H. Barnewitz and B. Stickan. "Improved Mesh Deformation". In: *Notes on Numerical Fluid Mechanics and Multidisciplinary Design*. Ed. by B. Eisfeld et al. Vol. 122. 2013, pp. 219–243.
- [38] G. A. Wilke. "Variable-Fidelity Methodology for the Aerodynamic Optimization of Helicopter Rotors". In: *AIAA Journal* (2019), pp. 1–14.
- [39] D. R. Jones et al. "Efficient Global Optimization of Expensive Black-Box Functions". In: *Journal of Global Optimization* 13 (1998), pp. 455–492.
- [40] A. Forrester et al. *Engineering Design via Surrogate Modelling: A Practical Guide*. Wiley, 2008.
- [41] D. G. Krige. "A Statistical Approach to Some Basic Mine Valuation Problems on the Witwatersrand". In: *Journal of the Chemical, Metallurgical and Mining Society of South Africa* 52.6 (Dec. 1951), pp. 119–139.
- [42] J. Roskam. *Airplane Design Part 1: Preliminary Sizing of Airplanes*. Lawrence, Kansas, USA: Design, Analysis and Research Corporation, 120 East Ninth Street, Suite 2, Lawrence, Kansas, 66044, USA, 1989.
- [43] D. P. Raymer. *Aircraft Design: A Conceptual Approach*. Third Edition. American Institute of Aeronautics and Astronautics, 1999.
- [44] L. R. Jenkinson et al. *Civil Jet Aircraft Design*. AIAA education series. American Institute of Aeronautics and Astronautics (AIAA), 1999.
- [45] J. D. Mattingly et al. *Aircraft Engine Design*. Second Edition. American Institute of Aeronautics and Astronautics, 2002.
- [46] L. M. Nicolai and G. Carichner. *Fundamentals of Aircraft and Airship Design*. Vol. 1. AIAA education series. American Institute of Aeronautics and Astronautics, 2010.
- [47] M.-H.-1.-3. Military. *Composite Materials Handbook, Polymer Matrix Composites: Materials Usage, Design, and Analysis*. Vol. 3 of 5. US Department of Defense, June 2002.
- [48] T. Bach and C. Hühne. "Structural Optimization of Stiffened Composite Panels for Highly Flexible Aircraft Wings". In: *12th World Congress of Structural and Multidisciplinary Optimization (WCSMO), Braunschweig, Germany*. Ed. by A. Schumacher et al. Springer, Cham, Jan. 2018, pp. 838–849.
- [49] T. F. Wunderlich. "Multidisziplinäre Optimierung von Flügeln für Verkehrsflugzeuge mit Berücksichtigung der statischen Aeroelastizität". PhD thesis. Technische Universität Braunschweig, Mar. 2013.
- [50] T. F. Wunderlich. "Multidisciplinary wing optimization of commercial aircraft with consideration of static aeroelasticity". In: *CEAS Aeronautical Journal* 6.3 (2015), pp. 407–427.